Solution Conformations of Wild-Type and Mutated Bak BH3 Peptides via Dynamical Conformational Sampling and Implication to Their Binding to Antiapoptotic Bcl-2 Proteins

Chao-Yie Yang,[†] Zaneta Nikolovska-Coleska,[†] Peng Li,[‡] Peter Roller,[‡] and Shaomeng Wang*[,†]

Departments of Internal Medicine and Medicinal Chemistry, University of Michigan, 1500 East Medical Center Drive, Ann Arbor, Michigan 48109-0934, and Laboratory of Medicinal Chemistry, National Cancer Institute, FCRDC, Building 376, Room 207, Fredrick, Maryland 21702

Received: July 11, 2003; In Final Form: November 14, 2003

The BH3 (Bcl-2 homology 3) domain of the Bcl-2 family of proteins plays a critical role in the regulation of programmed cell death, or apoptosis. A 16-residue peptide derived from the BH3 domain of the proapoptotic protein Bak potently binds to the antiapoptotic proteins Bcl-2 and Bcl-xL. While this Bak BH3 peptide adopts a well-defined helical conformation in the experimental NMR solution structure in complex with Bcl-xL, it does not adopt a stable helical conformation in water. Experimental structural determination of peptides without a stable and well-defined solution conformation remains a difficult task. In this paper, we investigated the solution conformations of this Bak BH3 peptide through extensive molecular dynamics (MD) simulations in water using a recently developed self-guided MD simulation (SGMD) method. Our simulations showed that the Bak peptide exhibits a partially formed helical structure with a fairly stable 6-residue helical segment at the N terminus and a less stable approximately 4-residue helical segment at the C terminus. Additionally, we also performed extensive SGMD simulations of two mutated Bak peptides, in which the arginine residue at position 5 is mutated to either an alanine or a glycine residue (R5A or R5G mutant) to investigate the influence of mutation on the solution conformations of the Bak peptide. We found that the R5G mutation greatly affects the solution conformations of the peptide, and the overall helix ratio decreases by a factor of 2 as compared to the wild-type Bak peptide. In contrast, the R5A mutation does not affect significantly the peptide solution conformations observed in the wild type. By use of a fluorescence-polarization-based binding assay, we quantitatively determined the binding affinities of these three Bak BH3 peptides to Bcl-xL protein. We found that the R5G and R5A mutants are 24 and 6 times less potent than the wild-type Bak peptide, respectively, suggesting that the helical ratio of the peptides is an important but not the only factor for their binding to Bcl-xL. Analysis of representative conformations of the R5A mutant suggested that the relatively stable helical segment close to the N terminus may greatly facilitate its binding to Bcl-xL.

Introduction

The Bcl-2 family of proteins plays a critical role in regulating programmed cell death or apoptosis.[1,2] This family of proteins consists of the antiapoptotic (antideath) members, such as Bcl-2 and Bcl-xL, and the proapoptotic (prodeath) members such as Bak, Bax, and Bad. The ability to form a heterodimer between the proapoptotic and the antiapoptotic members is crucial for their biological functions. The BH3 (Bcl-2 homology 3) domain of the proapoptotic members mediates their heterodimerization with the antiapoptotic proteins Bcl-2 and Bcl-xL. Indeed, individual peptides derived from the BH3 domain of Bad, Bak, Bid, and Bim potently bind to Bcl-2 and Bcl-xL proteins in vitro.[3] When fused with Antennapedia peptide, the Bak peptide was also shown to induce apoptosis in cancer cells.[4]

The interactions of BH3 peptides derived from proapoptotic proteins with Bcl-2 and Bcl-xL have been used as the model systems to probe the binding between proapoptotic and antiapoptotic Bcl-2 proteins. The three-dimensional (3D) solution structures of Bcl-xL in complex with the Bak (PDB ID: 1BXL)[5] and Bad (PDB ID: IG5J)[6] BH3 peptides have been solved by NMR methods. In these complex structures, Bak or Bad BH3 peptides adopt a well-defined helical structure and bind to the same hydrophobic groove of Bcl-xL proteins.[5,6] Although both Bak and Bad BH3 peptides adopt a well-defined helical conformation in the complex structure, they do not adopt a stable helical conformation in aqueous solution that can be studied reliably using conventional circular dichroism (CD) spectroscopy.[6] By use of the trifluoroethanol (TFE) as a helix-stabilizing agent, the 16-residue Bak BH3 peptide was shown to have 22% helix content, while the 25-mer Bad BH3 domain peptide exhibits 44% helix content in 30% TFE.[6] The 25-residue Bad BH3 peptide was also shown to bind to the Bcl-xL with an affinity nearly 1000 times better than the 16-residue Bak BH3 peptide.[6] The difference in their helix content has been suggested to be one major factor contributing to their binding affinity difference.[6] Note that the helix content experiments were performed in TFE/H_2O while the binding experiments were performed in aqueous solution.[6] The detailed structural information of these BH3 peptides in aqueous solution is still lacking, although such information is important for the understanding of their binding to Bcl-2 and Bcl-xL.

Traditional CD spectroscopy is commonly used to detect helix content of peptides or proteins. However, the CD measurement is only sensitive to the average properties of partial helical

[†] University of Michigan.
[‡] National Cancer Institute.
* Author to whom correspondence may be addressed. Phone: (734) 615-0362. Fax: (734) 647−9647. E-mail: shaomeng@med.umich.edu.

10.1021/jp036009f CCC: $27.50
Published on Web 01/03/2004

peptide and the optimal sensitivity is around 50% of the helix content.[7] Contribution of very short helical segments to the CD spectra is small,[8] which makes it difficult to detect short helical segments in solution using the traditional CD spectroscopy. Recently, a short helical segment consisting of four residues stabilized by a La^{3+} ion has been studied by Baldwin and coworkers using CD measurements.[9] They found a substantial helical CD spectrum for the short segment in contrast to the nonhelical prediction made based upon the standard equation used in CD measurement for the helix content calculation. Thus, substantial short helical segments may exist for the Bak BH3 peptide in solution, and identification of short helical segments from the Bak peptide by the traditional CD spectroscopy would be difficult.[6]

Computational molecular dynamics (MD) simulations thus provide an alternative method to study the solution conformations of the Bak BH3 peptide in aqueous solution at atomic resolution. Because the random coil−helix transition occurs on the order of 10−100 ns for helical peptides,[10,11] the time scale required to observe frequent coil−helix transitions using the conventional MD method could exceed 100 ns for the Bak peptide. Therefore, we use the recently developed self-guided molecular dynamics (SGMD)[12] with an enhanced conformational sampling as compared to the conventional MD method to expedite the conformational searching process. SGMD was shown to enhance the conformational sampling by a factor of up to 100 in liquid Argon crystallization.[13] This method has been used successfully to simulate the folding of turn, helix, and β-hairpin structures for several peptides.[12−15] To facilitate sampling in different conformational spaces and avoid bias to a particular conformational region, we performed independent simulations started from two different initial conformations. We also performed extensive SGMD simulations of two mutated Bak peptides (R5G and R5A) to investigate the effects of point mutation to the solution conformations of the Bak peptide. We have determined experimentally the binding affinities of these three Bak BH3 peptides to Bcl-xL using a sensitive and quantitative fluorescence polarization (FP) binding assay. On the basis of our simulation results and experimental binding affinity data for these Bak BH3 peptides, we discussed the importance of the solution conformations to the binding of the Bak peptides to Bcl-xL.

Method and Simulation Details

1. Simulation Setup. Details of the SGMD method and the implementation were described previously.[12] In this study, we have used the Amber program (version 6)[16] for all simulations except the free energy analysis. The force-field parameters used were from Cornell et al.[17] For SGMD, we have used an average time of 0.2 ps and the guiding factor of 0.2.

The sequence of the wild-type Bak peptide is GQVGRQLAI I GDDINR, which corresponds to the BH3 domain residues 72−87 in the Bak protein, which were renumbered as residues 1−16 in this paper. The extended conformation of the wild-type Bak was generated using the Sybyl program.[18] The peptide was first solvated with explicit water using the TIP3P model,[19] where the distance between the peptides and the edge of the water box was set to 10 Å. A 500-step minimization run and a 10-ps equilibration run at 300 K were performed with the peptide structure fixed to allow water molecules to diffuse into the void created during the initial setup. Another 200-ps equilibration run was performed for the whole system with the temperature of the system set at 300 K. Finally, the production run using SGMD for each peptide was carried out. For the initial helical conformation, the structure was extracted from the NMR structure of the Bak peptide in complex with Bcl-xL.[5] After the equilibration, a 2-ns conventional MD was run before conformational sampling using SGMD was performed.

Configurations of every 0.5 ps were saved and those of every 5 ps were used in the secondary-structure and free-energy calculations. All the MD simulations were NTP simulation ($T = 300$ K and $P = 1$ atm). The SHAKE algorithm[20] was used to fix the bonds involving hydrogen. The PME method[21] was used, and the nonbonded cutoff distance was set at 10 Å. The time step was 2 fs, and the neighboring pairs list was updated in every 20 steps.

In the mutated peptide simulation, single-site mutation of arginine at residue 5 into either R5A or R5G was made. Local side-chain minimization of the mutated residue was performed in Sybyl[18] before embedding the peptide in water.

2. Structural and Free-Energy Analysis. The DSSP algorithm from Kabsch and Sander[22] and the STRIDE algorithm from Frishman and Argos[23] were employed to analyze the secondary structural conformations of the peptides. In the DSSP algorithm, the predicted secondary structure was based on different patterns of the hydrogen bonds between peptide carbonyl and amide groups. Specifically, the hydrogen bond was defined by the distance criteria between carbonyl and amide groups whose electrostatic energy was less than a threshold value. The helix was assigned if at least two consecutive *n*-turns exist in the structure where *n* denoted the sequence number difference between the carbonyl and amide group. Thus, $n = 3$ is called a 3^{10}-helix, $n = 4$ is called an α-helix and $n = 5$ is called a π-helix. The minimum numbers of residues in 3^{10}-, α-, and π-helices are 3, 4, and 5. The second algorithm considered here is STRIDE, which was developed to narrow the gap of the disagreement between predictions made by the DSSP algorithm and crystallographers' assignments.[23] The STRIDE algorithm included different definitions of hydrogen bonds using distance and directional properties (angles) and torsional angle probability of the backbone dihedral angles for the recognition of secondary structures. In this study, because the π-helix appeared in less than 0.1% of conformations, it was not included in our secondary structural analysis. Only α- and 3^{10}-helices were included in the analyses. The short and quasi-stable helical segments observed in simulations cannot be identified using conventional CD measurements. To avoid confusion between our analyses with the standard helix content used in the CD spectra, we define the helix ratio as the number of residues in the helical segments predicted by the secondary structure identification algorithm divided by the total number of residues in the peptide in a conformation in our analysis.

The Carnal module in the Amber suite was used for the backbone-heavy atoms root-mean-squared deviation (RMSD) calculation where heavy atoms referred to N, C, Cα, and O atoms. The MM-PBSA module in the Amber program (version 7)[24] was used for the free-energy calculation. The charges and van der Waal radius were assigned using the Amber force-field 94 parameters.[17] Because the calculation of entropy is expensive, it is not considered in this study. The effective free energy used in this work can be broken down into the following terms, $G_{\text{eff}} = E(\text{MM}) + E(\text{solv})$, where $E(\text{MM}) = E(\text{internal strain}) + E(\text{nonbonding vdW}) + E(\text{nonbonding electrostatic})$ and $E(\text{solv}) = E(\text{polar}) + E(\text{nonpolar})$.

The terms in the E(MM) category are the internal strain energy, the nonbonding van der Waal interaction, and the nonbonding electrostatic interaction energy. The dielectric constant used in the E(MM) term is equal to 1. The polar

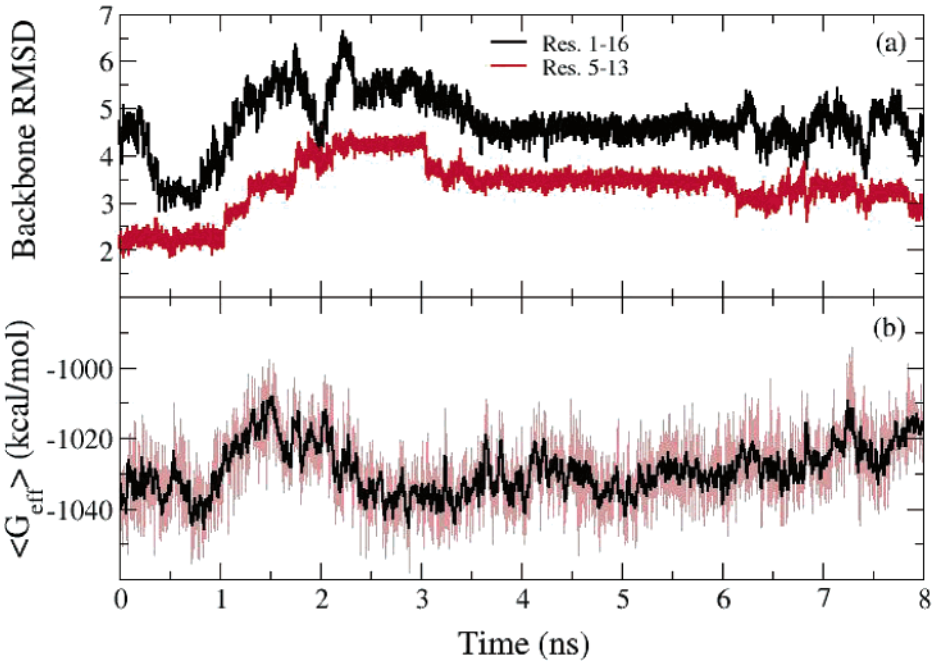

Figure 1. (a) All residues and backbone residues 5−13 RMSD in reference to the helical form NMR structure extracted from the complex from the initially helical form Bak peptide sampling. (b) The effective free energy of the conformations calculated using the MM-PBSA method. The thick line is a 10-point (or 50-ps) running average of the effective free energy.

solvation energy was calculated using the DELPHI program,[25] and the nonpolar solvation energy is linearly proportional to the accessible surface area (ASA), i.e., E(nonpolar) = 0.00542·ASA + 0.92 (kcal/mol).[26]

3. Peptide Synthesis. The three peptides were synthesized on an ABI 433A peptide synthesizer, starting with PAL amide resin for establishing the C terminal carboxamide and using the chemical protocols based on the Fmoc chemistry. After the elongation of the peptide chain, the resin-anchored linear peptide was cleaved from the resin by treatment with trifluoroacetic acid containing 2.5% each (v/v) of triethylsilane and deionized water for 2 h. Three-fourths of the cleavage solution was evaporated under N_2, and the remaining residue was precipitated and washed with ice-cold ether. The crude products were purified by reverse phase high-performance liquid chromatography using a Vydac C8 column (22 mm × 250 mm) with the following conditions: solvent system A, 0.05% TFA in water; solvent system B, 0.05% TFA in 90% acetonitrile in water; gradient, 10−53% B over 20 min; flow rate, 10.0 mL/min; UV detector set at 225 nm. The R_t values for R5G and R5A were 17.1 and 17.8 min, respectively. The final products were characterized and confirmed by fast-atom bombardment and/or matrix-assisted laser desorption ionization time-of-flight mass spectra.

4. Binding Assay. A sensitive and quantitative in vitro competitive binding assay based on the FP method was developed and used to determine the binding affinity of Bak peptide and two mutated Bak peptides (R5A and R5G) to Bcl-xL protein. For this assay, 6-carboxy fluorescein succinimidyl ester (FAM) coupled to the Bid peptide 21-mer (79−99) Flu-Bid, with high binding affinity to Bcl-xL protein (K_d = 3 nM), was used as the tracer. For Bcl-xL protein, we used the stable and soluble recombinant Bcl-xL protein fused to His-tag.

FP experiments were performed in Dynex 96-well, black, round-bottom plates (Fisher Scientific) using the Ultra plate reader (Tecan U. S., Inc., Research Triangle Park, NC). A 5-μL sample of the tested peptides, preincubated Bcl-xL (0.006 μM), and Flu-Bid (0.005 μM) in the assay buffer (100 mM potassium phosphate, pH 7.5; 100 μg/mL bovine gamma globulin; 0.02% sodium azide, purchased from PanVera Company) were added in the 96-well plate to produce a final volume of 125 μL. The contents in the plates were mixed and incubated at room temperature for 3 h to reach equilibrium. The IC50, i.e., the inhibitor concentration at which 50% of the protein-bound peptide is displaced, was determined by fitting the data points to the curve based on the standard equations via the nonlinear least-squares method using GraphPad Prism software. The K_i values were calculated using a modified Cheng−Pruff equation.

Results and Discussions

1. Conformational Analysis of the Wild-Type Bak Peptide Starting from the Initial Helical and Extended Conformation. We characterized the solution conformations of the Bak peptide during the simulations by analyzing (1) the backbone RMSD compared with a reference conformation, (2) the secondary structures, and (3) the effective free energy $\langle G_{eff} \rangle$ of the conformations. Each of these measures provides partial information about the peptide conformations at the atomic level. For example, the backbone RMSD indicates the deviation of the backbone topology of the conformations from the reference conformation. Secondary structure analysis shows the pattern of hydrogen bonds between the backbone atoms including helix, β-sheet, and β-turn where we focus on the helix pattern in this work. Besides the backbone topology inferred from the above two measures, the $\langle G_{eff} \rangle$ provides the energetic stability information of the peptide conformation contributed from both the intramolecular (E(MM)) and the intermolecular (E(solv)) interactions.

Starting from the linear helical Bak peptide conformation extracted from the solution complex structure with the Bcl-xL protein solved by NMR, we can sample the conformational states of the Bak peptide close to its bound form with Bcl-xL protein. In the beginning, we have run a 2-ns conventional MD simulation without using SGMD and observed an increase of backbone RMSD from 2 to 4 Å in reference to the linear helical Bak peptide conformation (data not shown). After we started the SGMD simulation, we found a decrease of backbone RMSD

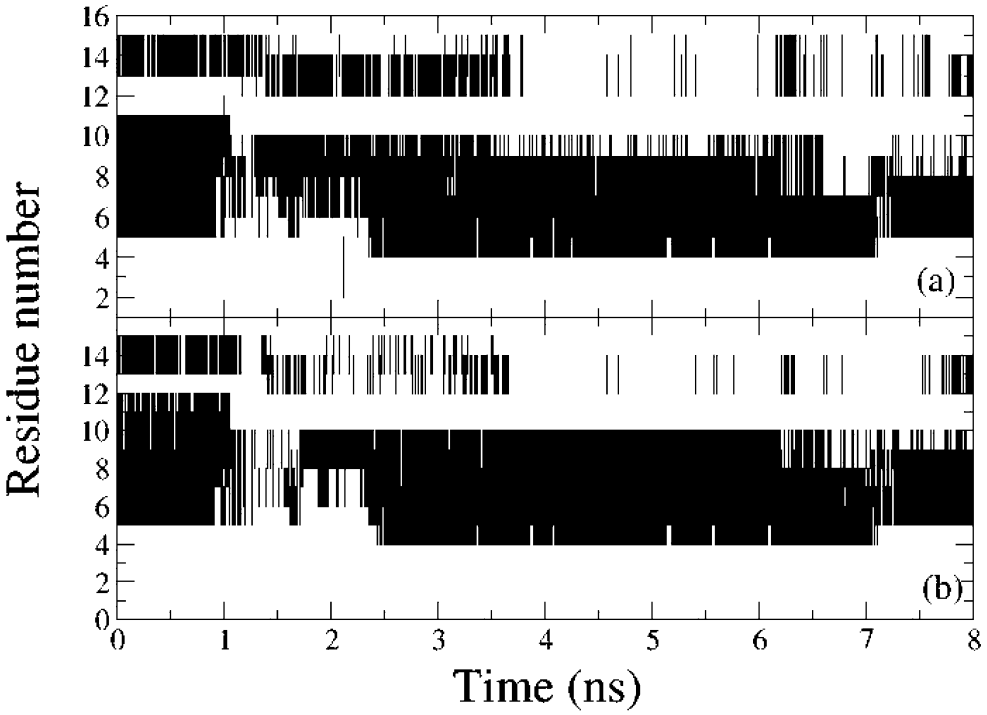

Figure 2. Helical segments formation from the initial linear helical Bak peptide conformation sampling based on (a) DSSP and (b) STRIDE.

to 3 Å initially (black line from 0 to 0.8 ns in Figure 1a). If we used only residues 5−13 (the location of the helix in the Bak peptide from the complex NMR structure), we found a smaller backbone RMSD value of 2 Å in the same time period (red line in Figure 1a). The results from the simulation before 1 ns in Figure 1 showed that the backbone helical structure between residues 5−13 is stable when the Bak peptide was trapped in the conformational space close to the bound form and also assured that our dynamical sampling method introduced small perturbations to the underlying molecular mechanics force field. The sampling of different conformational space started to occur after 1 ns in Figure 1, evidenced by the rise of the backbone RMSD using either all residues or residues 5−13 as measures. Between 4 and 6 ns, the backbone topology of the peptide remains stable where the RMSD measures using either residues 1−16 or 5−13 are both maintained at 4.5 and 3.5 Å, respectively, with small fluctuations. When inspecting the $\langle G_{\text{eff}} \rangle$ in Figure 1b, we observed less dramatic variation than RMSD measures in Figure 1a except for the time window between 1 and 2.5 ps. Similarly, the conformations between 4 and 6 ns exhibit relatively small fluctuation in $\langle G_{\text{eff}} \rangle$. The large deviation of RMSD and relative smaller variation in $\langle G_{\text{eff}} \rangle$ suggests that the backbone hydrogen bonds contribute only a smaller portion of stabilization to the peptide conformation for the conformational space sampled here.

In the secondary structure analysis for identifying helical segments, we used the DSSP and the STRIDE algorithms and results are plotted in Figure 2. Both algorithms predicted similar locations of helical segments in each conformation, and two helices exist in the conformations at the beginning of the sampling. In addition, both algorithms predicted that the helical segment from residues 4−10 is stable from 2.5 to 6 ns. Small differences in the helical segment prediction exist among the two algorithms. For example, less helical segments were predicted by STRIDE between 1.5 and 3.5 ns and the DSSP algorithm predicted less helical involvement of residue I10 between 3.5 and 6 ns. Because of the similar results obtained by these two algorithms and the fact that DSSP is more widely used, we use the DSSP algorithm for the helix ratio analysis in the following sections. We anticipate the differences of helical-segment prediction between these two algorithms are minimal for the Bak peptides studies in this paper.

From the 8-ns SGMD simulation discussed above, it is clear that the helix from R5 to D13 found in the complex between Bak peptide and Bcl-xL protein breaks into one long and one short helical segment in the simulation. Combination of the analysis of the backbone RMSD, $\langle G_{\text{eff}} \rangle$, and stability of the helical segment (see Figures 1 and 2) suggested that the conformations between 4 and 6 ns (denoted HST1) represent a quasi-stable state of the Bak peptide.

After our discussion of the conformational space sampling of the Bak peptide close to its bound form with the Bcl-xL protein, we now turn to a different initial condition in the simulation. Here, we started the simulation by assuming that the Bak peptide takes the hypothetical extended conformation. By use of the unbiased backbone conformation for the initial condition, we performed a longer conformational sampling simulation (35 ns). Because the bound form of the Bak peptide with Bcl-xL protein is not the native solution conformation of the Bak peptide, we do not anticipate the conformations sampled here will resemble the bound-form Bak peptide. We therefore did not perform the backbone RMSD comparison in reference to the bound-form Bak peptide as our previous simulation and used other measures including energy and secondary structure assignments to characterize the conformations of the Bak peptide in the simulation.

In Figure 3a, we displayed the effective free energy $\langle G_{\text{eff}} \rangle$ for the conformations from the 35-ns conformational sampling using the initial extended conformation of Bak peptide. The variation of $\langle G_{\text{eff}} \rangle$ spans over 36 kcal/mol (from −1040 to −1004 kcal/mol).[27] When we used the average of $\langle G_{\text{eff}} \rangle$ between 4 and 6 ns in Figure 1b (−1031.0 kcal/mol) as a guide line, we found that the conformations in 7−9 ns (denoted ETST1) and 30−33 ns (denoted ETST2) have lower $\langle G_{\text{eff}} \rangle$ than HST1 and the stability of these conformations also sustained for about 2−3 ns. The frequent transitions between the low energy states in

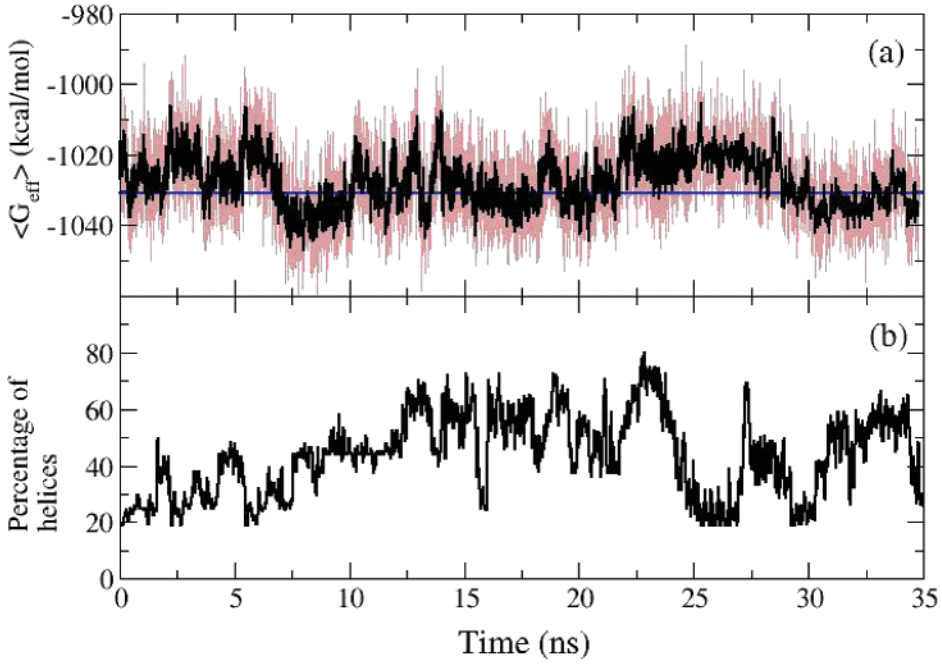

Figure 3. (a) Effective free energy of the conformations from the sampling simulation started with the extended conformation. The horizontal line is the averaged reference energy from Figure 1b from 4 to 6 ns. The thick line corresponds to the 10-point (50-ps) running average. (b) The 10-point (50-ps) running average of the percentage of helices in each conformation.

Figure 3a are characteristic of SGMD simulation and are indications of the peptide-surmounting conformational barriers during the sampling. Because the backbone hydrogen bonds were typically used in the protein-folding simulation for identifying stable microstates,[28] we also investigate the role of the backbone hydrogen bonds in the stability of the peptide solution conformations by calculating the total percentage of helical segments in these conformations predicted by the DSSP algorithm and correlated them with $\langle G_{\text{eff}} \rangle$. In Figure 3b, we found that 20% of the helix ratio forms at the beginning of the sampling and the helix ratio varies between 20 and 60% during the entire 35-ns simulation. No direct correlation between high percentage of helices and low $\langle G_{\text{eff}} \rangle$ values was observed for this 16-residue peptide. For example, an ensemble of the lowest $\langle G_{\text{eff}} \rangle$ value (7−9 ns) exhibited 40% of the helix ratio while the second to the lowest ensemble (30−33 ns) showed 60% of the helix ratio. However, we found that conformations with 40% of the helix ratio sustained for 5 ns (from 7 to 12 ns) in Figure 3b. The variation of the helix ratio between 20 and 60% observed in our simulation is another indication of the disordered nature of Bak peptide in solution. Simulations from different initial conformations presented here indicate that backbone hydrogen bonds play a smaller role in the stability of the Bak peptide solution conformations.

In Figure 4, we display the location of the helical segments in the 35 ns. Many short helices consisting of 3−4 residues in length were identified in most conformations, and two to three helical segments were constantly observed in a single conformation. Although the percentage of the helical segment plotted in Figure 3b appears to be higher than the experimental measurement at first glance, the high percentage results from the existence of more than one short helical segment in the Bak peptide in water from our simulation demonstrated in Figure 4. These relatively short-lived and short helical segments observed in the conformations from our simulation may be difficult to detect using conventional CD measurements. Furthermore, different patterns of helical segment location can be seen in Figure 4 among the quasi-stable states identified previously. For examples, we found one stable helix from Q2 to A8/I10 in ETST1, two separated helical segments in ETST2. Only ETST1 showed similar helix location to that found in HST1 (cf. Figure 2). The secondary structure analysis of these quasi-stable states was used to calculate the helical propensity of each residue, which are compared with another independent measure discussed later in the paper.

As mentioned earlier, the helix content reported in CD measurements usually shows no details of the number of separated helices or the population of different helix content in the conformations. To provide the detailed information on the helix ratio and the location of the helical segments in the conformations obtained from our simulations, we calculated the distribution of the helix ratio, the distribution of the residue length in each helical segment, and the helical propensity of each residue for each conformation obtained from the two simulations started with two different initial conformations. In the conformations obtained from the simulation started from the linear helical conformation, peaks of distribution in the helix ratio are found mostly in 20, 40, and 60% in Figure 5a. The percentage of population with 60% is decreased by a factor of 2 for conformations obtained from the simulation started with the extended conformation. Conformations with a helix ratio greater than 60% are also observed with a much smaller percentage of population when started with the initial extended conformation. The data indicated that 40% of the helix ratio (about 6 residues for the 16-mer Bak peptide) is dominant in both simulations.

The dominant 40% of the helix ratio for the peptide obtained from the simulations does not show the number of helical segments in the peptide. To address this issue, we calculated the distribution of the residue length in each helix in Figure 5b and correlated the data with Figure 5a. In this calculation, if a conformation consists of 3 helices, it will be treated as three independent helical segments in this statistical analysis. Clearly, the dominant distribution of the residue length in a helical segment is 3−4 residues and the second dominant population involves 6−7 residues. Therefore, the dominant 40% of the helix

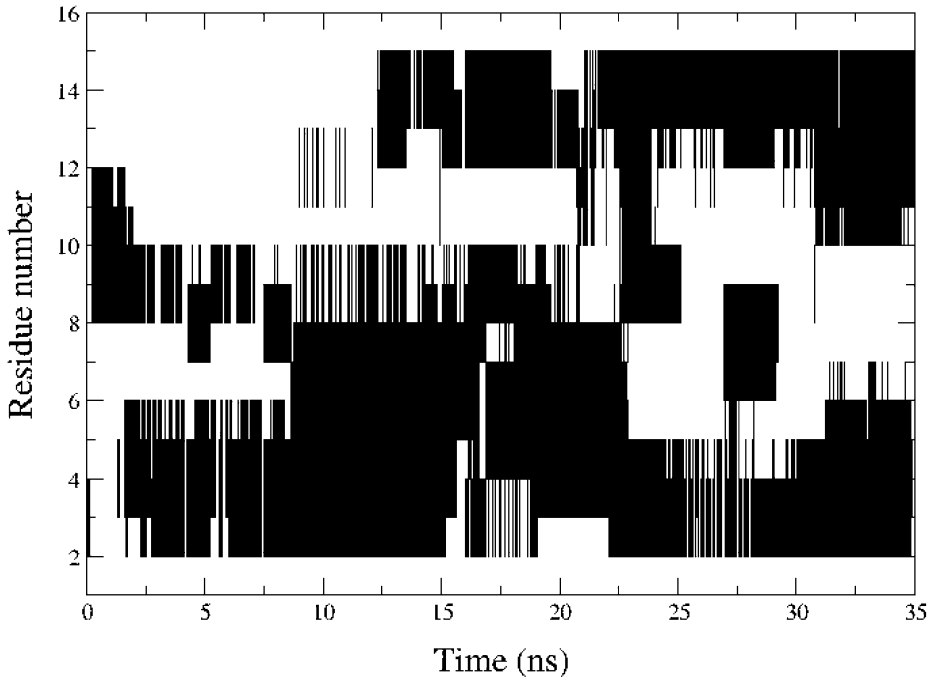

Figure 4. Helical segments formation from the Bak peptide sampling simulation started with the extended conformation.

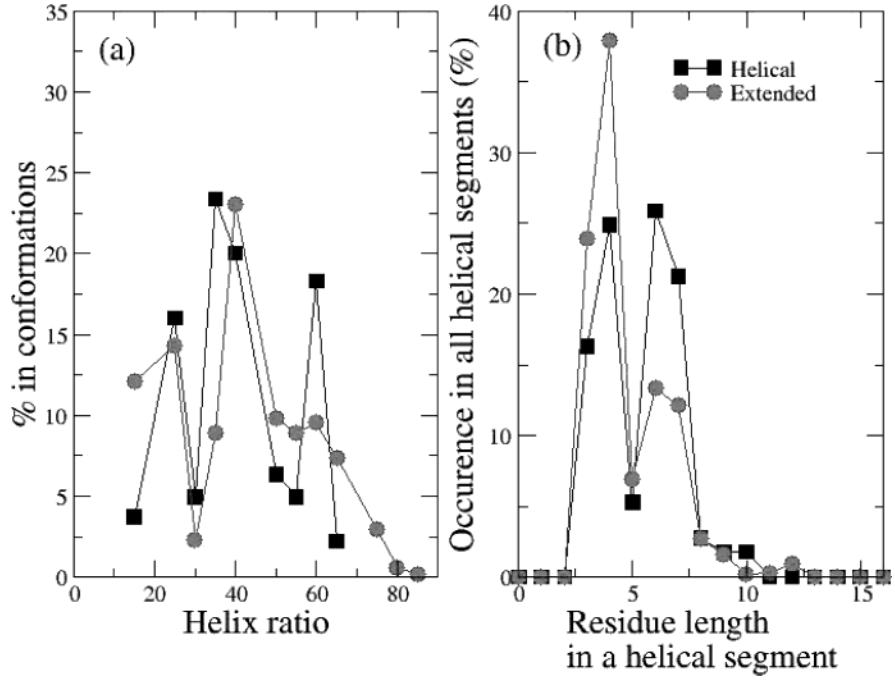

Figure 5. (a) Helix ratio vs the percentage population in the conformations from the helical and extended Bak peptide conformational sampling. (b) Distribution of residue length in a helical segment from the helical and extended Bak peptide conformational sampling.

ratio in a single conformation found in Figure 5a is the result of the existence of either one helical segment with 6−7 residues or two short helical segments. The analysis of the helix length distribution quantitatively confirmed the existence of fairly short helical segments in the solution conformation of the Bak peptide, irrespective of which initial conformations were used in the simulation.

Besides the distribution of the helix ratio, the helical propensity of each residue observed from different conformations shows the probable location of helices in the amino acid sequence. In Figure 6, we calculated the helical propensity of each residue from both simulations, i.e., the linear helical and extended conformations, by including all conformations in Figure 6a and conformations of HST1, ETST1, and ETST2 only in Figure 6b. Figure 6a showed that the Bak peptide tended to form two helices, one long helical segment close to the N terminus and one short helical segment close to the C terminus when started from either the linear helical or extended conformation. Small differences exist in these two simulations, such as that Q2 and V3 residues exhibit higher helical propensity when started from the extended conformation. However, both simulations showed very low helical propensity at G11. As for the three quasi-stable states in Figure 6b, both HST1 and ETST1 ensembles agreed fairly well with each other where very low helical propensity from I10 to R16 and high propensity from Q2 or G4 to I9 were found. The ensemble from ETST2 is different from HST1 and ETST1 in that residues close to both termini are higher in helical propensity than those in the middle.

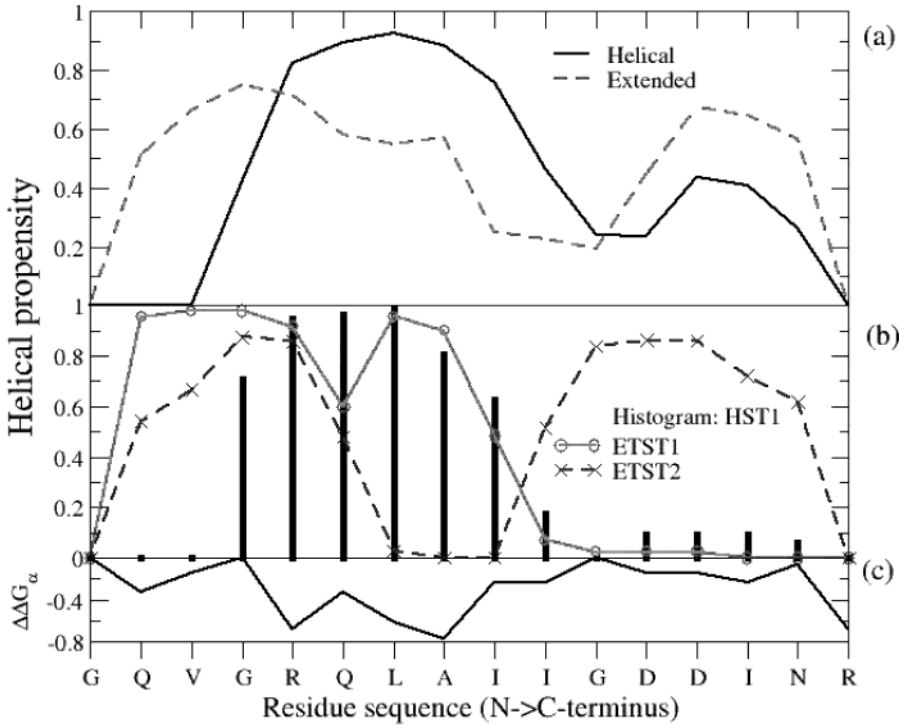

Figure 6. (a) Helical propensity based on all conformations from the conformational sampling of the initial helical and extended conformations. (b) Helical propensity based on three energetically quasistable states, i.e., HST1, ETST1, and ETST2. (c) Differences in the free energies of helix stabilization data for each residue from O'Neil and DeGrado.[29]

The similarity in the helical propensity between these two simulations suggests that sufficient sampling may have been achieved for the purpose of secondary structural analysis.

We also compared the helical propensity calculation in Figure 6b with a different independent measure reported by O'Neil and DeGrado[29] in Figure 6c. They determined the free-energy difference of each residue ($\Delta\Delta G_\alpha$) in stabilizing the helix conformation using a guest system.[29] The more negative $\Delta\Delta G_\alpha$ correlates with the higher helical propensity predicted to be seen in an equilibrium system for that residue. The $\Delta\Delta G_\alpha$ data should be compared with the quasi-stable states which correspond to a quasi-equilibrium system in the simulation. Note that the values of the N- and C-terminus residues plotted here are only for the purpose of completeness because the experiments did not consider the terminal residues. From the comparison, we found that the helical propensity estimate from the HST1 (histogram in Figure 6b) agrees favorably with the experimental measurement (Figure 6c), suggesting that the ensemble of HST1 is one of the quasistable states. Although the ensemble represented by ETST1 overestimates the helical propensity at Q2 and V3, the conformations of ETST1 were energetically lower than those of HST1, partially due to the stabilization by their longer helical segments. Therefore, we believe ETST1 is also a quasistable state. As for ETST2, no direct correlation between simulation and experimental data is found regarding the helical propensity and may represent a transient quasistable state.

2. The Effect of Single-Site Mutation to the Helical Formation. A point mutation in the Bak peptide can impact its binding to Bcl-2 and Bcl-xL proteins by affecting its solution conformations and/or its direct interactions with the proteins. In this paper, we focused on two mutants where the arginine residue at position 5 is mutated into either an alanine (R5A mutant) or a glycine (R5G mutant). In the NMR solution structure of the Bak peptide in complex with Bcl-xL, this arginine residue is exposed to solvents and appears to have no direct short-range interactions with the protein, although it is possible that the arginine residue may have long electrostatic interactions with the protein. Therefore, Arg5 is an ideal candidate residue to make a single point mutation to probe the effect of the solution conformations of the peptide on the binding of Bak peptide to Bcl-xL without severely affecting short-range interactions between the Bak peptide and Bcl-xL protein. We performed a 10-ns SGMD simulation on each of these two mutants in water started from an extended conformation and compared them with the wild-type Bak peptide simulation to address this issue.

From the 10-ns SGMD simulations, the magnitude of changes in $\langle G_{\text{eff}} \rangle$ between the initial and the lowest $\langle G_{\text{eff}} \rangle$ conformations for both mutants are similar to the wild type, i.e., about 50 kcal/mol (Figure 7). The location of helical segments for the wild type and mutants were plotted in Figure 8. Note that all these simulations were started with the extended conformations and followed the same simulation protocol. In Figure 8, significantly less helical segments were found for the R5G mutant while more helices appeared for the R5A mutant during the 10-ns SGMD simulations. The averaged helix ratio for the wild-type Bak peptide, the R5A mutant, and the R5G mutants in the 10-ns simulations were 31, 38, and 14%. In the wild-type Bak peptide simulation, short helical segments formed frequently until 8.5 ns when a longer helix from residues 2−8 became stable. In the R5G mutant simulation, less short helical segments appeared and a longer helix formed for a shorter time period (1 ns). As for the R5A mutant, the long helix from residues 3−10 formed earlier in the simulation and was sustained for 4 ns. Figure 8 also showed that the single-site mutation affected the helix formation in other location of the peptide in the R5G mutant, namely, the short helix close to the C-terminus from D13 to N15 found for the wild-type and the R5A mutant did not form in the R5G mutant.

For a quantitative illustration of the effects of mutation on each residue, we plotted the helical propensity for each residue in Figure 9 using conformations from the 10-ns simulations for

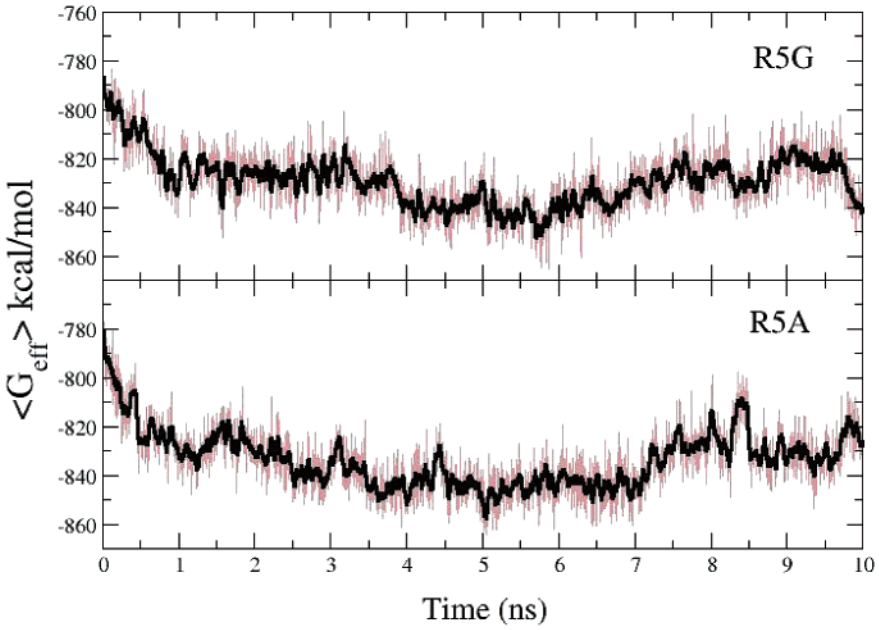

Figure 7. Effective free energy from the trajectories of R5G and R5A mutants simulations.

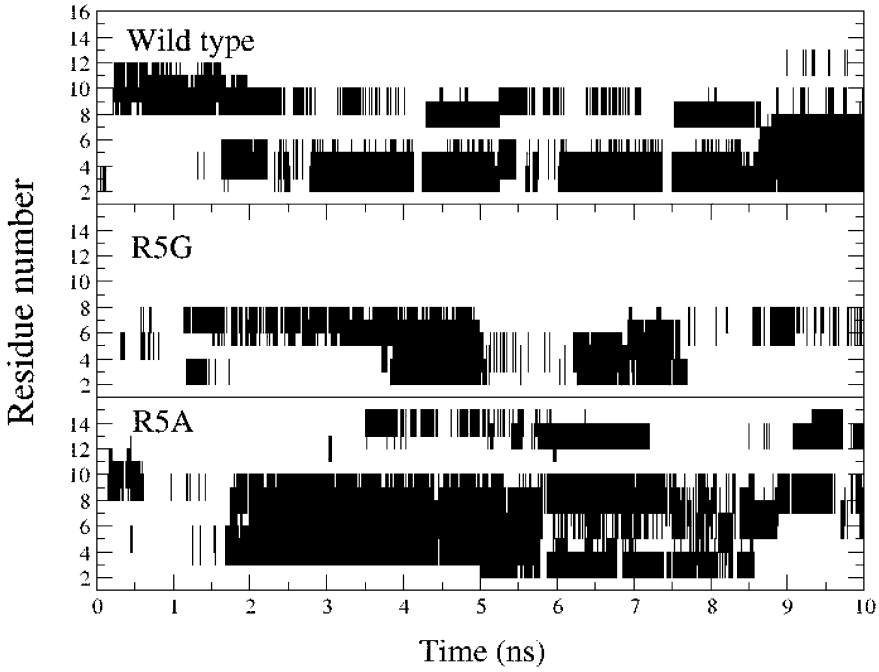

Figure 8. Location of helical segments in the 10-ns wild-type and R5G and R5A mutated Bak peptides simulations predicted by DSSP algorithm.

these three peptides. Although the trajectories are shorter than the 35-ns simulation for the wild-type Bak peptide started from the extended conformation, we already observed significant effects of mutation to the helical propensity. In the R5G mutant, the helical propensity of the residues close to the N-terminus decreases by a factor of 2 and no helical propensity was observed for the short helical segment close to the C terminus. In contrast, in the R5A mutant, the helical propensities of the residues close to N terminus are similar, with a highest propensity shifted from V3 in wild type to A8 in R5A. Most notably, the stabilization of the short helix close to the C-terminus is evident for the R5A mutant. Significantly, we observe that the single point mutation at Arg5 affects not only the local helical propensity trend but also the overall helical propensity for each residue in the peptide. The similarity of helical location between the wild type and R5A mutant suggests little change in the backbone topology between them in solution. The low helical conformations of the R5G mutant observed from our simulation predict that this mutant may bind to Bcl-xL with much lower affinity than the wild-type Bak peptide, as confirmed with our experimental data discussed in the next section.

3. Experimental Determination of the Binding Affinities of the Wild-Type Bak Peptide and Two Mutants, R5A and R5G, to Bcl-xL. To experimentally determine the effect of single-site mutation to the Bak peptide on its binding affinity to the Bcl-xL protein, we have synthesized the wild-type Bak peptide and R5A and R5G mutants and quantitatively determined their binding affinity to Bcl-xL using a sensitive and quantitative FP-based binding assay. The wild-type Bak peptide and the R5A mutant have K_i values of 0.28 and 1.83 μM, respectively (Figure 10), in good agreement with the published

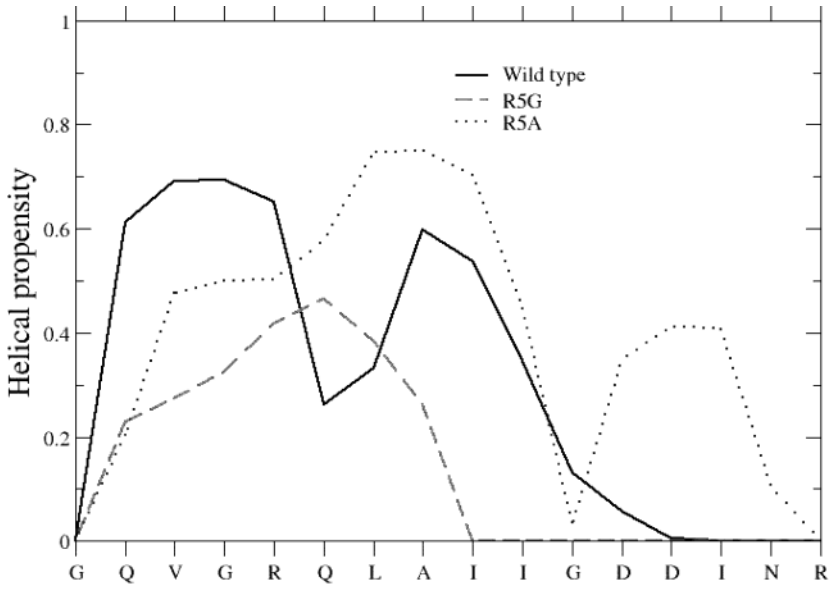

Figure 9. Effects of mutation on the helical propensity from the 10-ns wild type and R5G and R5A sampling simulations.

results.[5,6] We obtained a K_i value of 6.48 μM for the R5G mutant (Figure 10). Therefore, the R5A and R5G mutants are 6 and 24 times less potent than the wild-type Bak peptide in its binding to the Bcl-xL protein. The reduction in each case cannot be associated only with the reduction in the helical properties of the peptides because our simulation indicated the R5A mutant and the wild-type Bak peptide have similar helical conformations in solution. If the helix ratio is the sole determining factor for the potency, we would anticipate a similar binding affinity between the R5A mutant and the wild-type Bak peptide (38 vs 31% averaged helix ratio from the 10-ns simulations). The moderate reduction between the R5A and R5G mutants (a factor of 4) observed in experiments can be mostly accounted for by the differences in their averaged helix ratio from the 10-ns simulations (a factor of 2.7). However, the 6-times difference in the experimentally determined binding affinity between the R5A mutant and the wild-type Bak peptide led to the hypothesis that although arginine residue at position 5 does not have direct short-range interactions with the Bcl-xL protein, it may contribute to the binding of the wild-type Bak peptide to Bcl-xL through long-range interactions.

4. The Representative Conformations of the Wild-Type and Mutated Bak Peptides from Simulations and Implication to Their Binding with Bcl-xL Protein. In one of the current models for protein−protein interaction, it was proposed that the binding partners are initially guided by hydrophobic interaction.[31,32] The stabilization of the complex by the formation of salt bridges and hydrogen bonding between binding partners plays a role at a later stage of binding. The complex structure between the Bak peptide and Bcl-xL protein also showed that the hydrophobic interaction is one of the most important stabilizing factors to their binding.[5,33,34] In the Bak peptide, there are six hydrophobic residues with extended side-chain atoms and only V3, L7, I10, and I14 exhibit more than 40-fold reduction to the binding affinity in the alanine scanning analysis.[5] The largest change is from the L7A mutation.[5] From the secondary structure perspective, the above four hydrophobic residues are separated by 3−4 residues and the alignments of the side chains from these four residues are almost in parallel with each other when the peptide takes linear helical form. Thus, the linear helical form of the Bak peptide conformation not observed in solution is likely stabilized by the linear hydrophobic

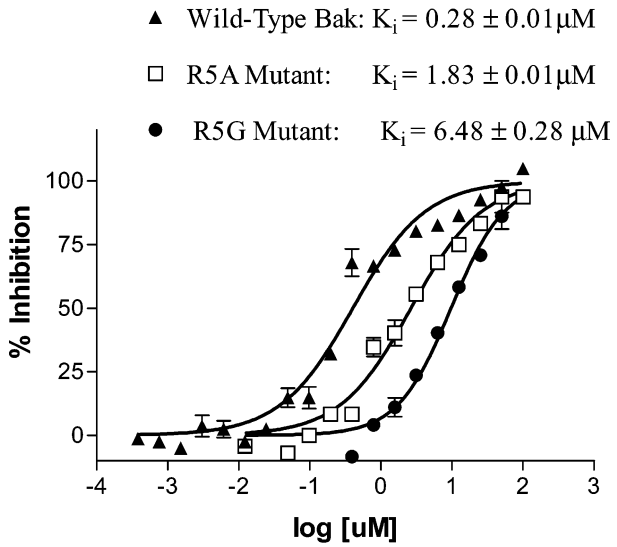

Figure 10. Competition binding curves of wild-type Bak peptide and two mutated peptides, R5A and R5G, with the Bcl-xL protein. Each data point was measured in triplicate and presented as the average ±SD. The IC50 of investigated peptides were determined by their ability to displace the fluorescent Bid 21-mer peptide from the Bcl-xL protein using the FP-based competitive binding assay. GraphPad Prism was used for nonlinear least squares curve-fitting.

groove provided by the Bcl-xL protein.[33,34] Because the alignment of the side chains from the four hydrophobic residues is strongly influenced by the location of the backbone helical segments, we therefore illustrate representative conformations from our simulations to discuss the common features and differences in the structures of the solution conformations of the Bak peptide and implication to their binding to the Bcl-xL protein.

To select the representative solution conformations of the wild-type Bak peptide from our simulation, we performed a cluster analysis[36] on all the conformations from the 35-ns simulation started with the extended conformation using the backbone torsion angles, which directly determine the backbone topology of the conformation. In the cluster analysis, we found 14 cluster groups and the conformations of the peptide corresponding to the center of each cluster group are drawn in Figure 11. In Figure 11, the population of each cluster group decreases

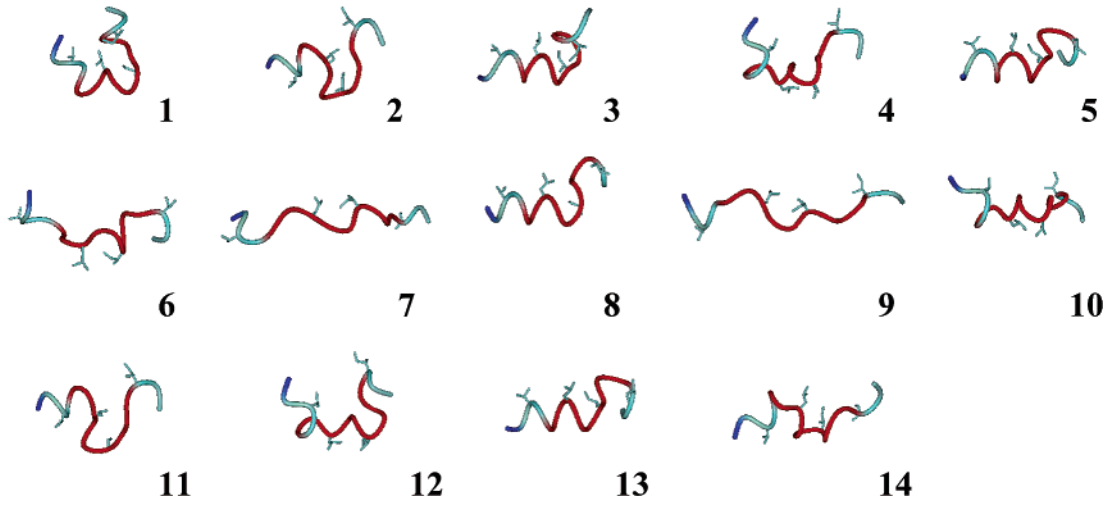

Figure 11. Fourteen representative conformations from the cluster analysis using the backbone torsional angles of the peptide. Each conformation is the center of each cluster group, and the population in each cluster group decreases from group 1 to 14. The blue- and red-color residues correspond to the locations of residues G1 and R5-D13. Four key hydrophobic residues (V3, L7, I10, and I14) are displayed in the figure as well. The pictures were prepared using the DINO program.[35]

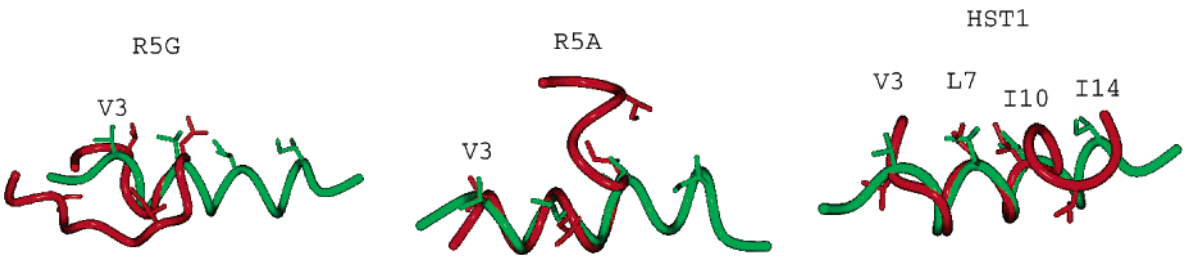

Figure 12. Superposition between helical form NMR structures (colored red) and the averaged structures (colored green) of R5G at 5.65 ns, R5A at 5 ns, and HST1 in the mutation simulations. Orientation of the side chains of V3, L7, I10, and I14 (from left to right) are drawn for comparison. The pictures were prepared using DINO program.[35]

from group 1 to 14. On the basis of the backbone topology, groups 6, 7, and 9 belong to random coil conformations and groups 2, 4, 10, 11, 12, and 14 belong to disordered conformations where short helical segments can be found. Groups 3, 5, 8, and 13 are similar in that at least one helical segment close to the N terminus is formed and V3, L7, and I10 are aligned accordingly. Although the most populous cluster group (group 1) did not show a well-formed helical segment close to the N terminus, V3, L7, and I10 are still aligned in a parallel pattern approximately. The number of conformations in groups 1, 3, 5, 8, and 13 accounts for 48% of the total conformations.

To illustrate the effect of mutation on the alignment of the four hydrophobic residues, we chose the averaged structure of 250 ps at 5.65 and 5 ns in the R5G and R5A sampling simulations for discussions. These structures are also the energetically lowest conformations in the simulations (see Figure 7). The R5A mutant exhibits similar topology and alignment pattern to cluster groups 3, 5, 8, and 13 (cf. Figures 11 and 12) and HST1. In contrast, the R5G conformation is in a disordered form and does not align well with the linear helical conformation seen in the NMR complex structure. The greater deviation of the R5G from the wild-type Bak peptide NMR structure suggests that a major conformational change is needed for the R5G mutant to bind to Bcl-xL, which may also contribute to its lower affinity to Bcl-xL than to the R5A mutant and the wild-type Bak peptide.

Taken together, our results suggest that although the Bak peptide does not adopt a linear helical conformation in aqueous solution, partially formed helical segments are found and may help to position the side chains of most of the key hydrophobic residues in parallel, which play an important role for the initial docking between the Bak peptide and Bcl-xL.

Conclusion

We have performed conformational sampling of the Bak peptide in explicit water using the SGMD method started with two different initial conformations. We frequently observed a helical segment consisting of 6−7 residues close to the N terminus and a less stable shorter segment of 3−4 residues close to the C terminus. Analysis of the distribution of the helix ratio showed a dominant 40% of the helix ratio (6−7 residues in length) for the Bak peptide in our simulations. The most probable number of residues in a helix found is 4, and the second most probable is 6. Therefore, the dominant 40% of the helix ratio in all the conformations identified from our simulations result from the presence of either a 6-residue helix or two separated short helices in a single conformation. These relatively short and quasi-stable helical segments may be difficult to identify in traditional CD experiments. Other experimental means, such as IR absorption of the amide-I vibration and NMR experiments,[38] may be used to confirm our findings. Although the R5A mutation does not affect the trend of the helical propensity observed for the wild-type Bak peptide significantly, the R5G mutation has a profound effect on the helical conformations of the Bak peptide in solution. Our binding experiments also showed that although the R5A mutant is only 6 times less potent than the wild-type Bak peptide binding to Bcl-xL, the R5G mutant is 24 times less potent than the wild-type Bak peptide binding to Bcl-xL. The 4 times reduction in binding affinity between R5G and R5A is attributed to the

decrease in the averaged helix ratio observed in simulation (2.7 times less). However, the 6 times reduction in the binding affinity between R5A and the wild type cannot be explained by the similar average helix ratio found in simulations. Both of our simulation and experimental results indicate that the reduced overall helical conformation for the R5G mutant contributes to its weak binding to Bcl-xL, although it is not the only factor, as indicated by the weaker binding affinity of the R5A mutant to Bcl-xL than that of the wild-type Bak peptide.

The 14 representative conformations from the cluster analysis also show that at least one partially formed helical segment close to the N-terminus in the conformations is common. This helical segment leads to a peptide conformation with side chains of V3, L7, and I10 aligned in a parallel orientation. The averaged structure from the low-energy ensemble of the R5A mutant shows similar backbone topology when compared to cluster group 3, 5, 8, and 13 and HST1 from the wild-type peptide simulations. In contrast, mutation of Arg5 to Gly results in a disordered backbone structure as evidenced from the averaged structure of the energetically favorable ensemble in the sampling. Taken together, our studies provide atomic detailed information of the solution conformations of the Bak BH3 peptide and its two mutants and the implications of the solution conformations to the binding of these peptides to Bcl-xL.

Acknowledgment. We would like to thank Dr. Judith Varady for her useful suggestions and comments and Karen Kreutzer for her excellent assistance.

References and Notes

(1) Adams, J. M.; Corey, S. *Science* **1998**, *281*, 1322.
(2) Corey, S.; Adams, J. M. *Nature Cancer Rev.* **2002**, *2*, 647.
(3) Letai, A.; Bassik, M. C.; Walensky, L. D.; Sorcinelli, M. D.; Weiler, S.; Korsmeyer, S. J. *Cancer Cell* **2002**, *2*, 183.
(4) Holinger, E. P.; Chittenden, T.; Lutz, R. J. *J. Biol. Chem.* **1999**, *274*, 13298.
(5) Sattler, M.; Liang, H.; Nettesheim, D.; Meadows, R. P.; Harlan, J. E.; Eberstadt, M.; Yoon, H. S.; Shuker, S. B.; Chang, B. S.; Min, A. J.; Thompson, C. B.; Fesik, S. W. *Science* **1997**, *275*, 983−986.
(6) Petros, A. M.; Nettesheim, D. G.; Wang, Y.; Olejniczak, E. T.; Meadows, R. P.; Mack, J.; Swift, K.; Matayoshi, E. D.; Zhang, H.; Thompson, C. B.; Fesik, S. W. *Protein Sci.* **2000**, *9*, 2528−2534.
(7) Rohl, C. A.; Baldwin, R. L. *Biochemistry* **1997**, *36*, 8435.
(8) Bierzynski, A. *Acta Biochim. Pol.* **2001**, *48*, 1091.
(9) Chin, D.-H.; Woody, R. W.; Rohl, C. A.; Baldwin, R. L. *Proc. Natl. Acad. Sci. U. S. A.* **2002**, *99*, 15416.
(10) Williams, S.; Causgrove, T. P.; Gilmanshin, R.; Fang, K. S.; Callender, R. H.; Woodruff, W. H.; Dyer, R. B. *Biochemistry* **1996**, *35*, 691.
(11) Thompson, P. A.; Eaton, W. A.; Hofrichter, J. *Biochemistry* **1997**, *36*, 9200.
(12) Wu, X.; Wang, S. *J. Phys. Chem. B* **1998**, *102*, 7238.
(13) Wu, X.; Wang, S. *J. Chem. Phys.* **1999**, *110*, 9401.
(14) Wu, X.; Wang, S. *J. Phys. Chem. B.* **2000**, *104*, 8023.
(15) Wu, X.; Wang, S.; Brooks, B. R. *J. Am. Chem. Soc*. **2002**, *124*, 5282.
(16) Pearlman, D. A.; Case, D. A.; Caldwell, W. S.; Ross, W. S.; Cheatham, T. E., III; DeBolt, S.; Ferguson, D.; Seibel, G.; Kollman, P. A. AMBER, a package of computer programs for applying molecular mechanics, normal-mode analysis, molecular dynamics, and free-energy calculations to simulate the structural and energetic properties of molecules. *Comput. Phys. Commun*. **1995**, *91*, 1.
(17) Cornell, W. D.; Cieplak, P.; Bayly, C. I.; Gould, I. R.; Merz, K. M., Jr.; Ferguson, D. M.; Spellmeyer, D. C.; Fox, T.; Caldwell, J. W.; Kollman, P. A. *J. Am. Chem. Soc.* **1995**, *117*, 5179.
(18) Sybyl, a molecular modeling system, is supplied by Tripos, Inc., St. Louis, MO 63144.
(19) Jorgensen, W. L.; Chandrasekhar, J.; Madura, J. D.; Impey, R. W.; Klein, M. L. *J. Chem. Phys.* **1983**, *79*, 926.
(20) Rychaert, J. P.; Ciccotti, G.; Berendsen, H. J. C. *J. Comput. Phys*. **1997**, *23*, 327.
(21) Darden, T. A.; York, D. M.; Pedersen, L. *J. Chem. Phys.* **1993**, *98*, 10089.
(22) Kabsch, W.; Sander, C. *Biopolymers* **1983**, *22*, 2577.
(23) Frishman, D.; Argos, P. *Proteins* **1995**, *23*, 566.
(24) Case, D. A.; Pearlman, D. A.; Caldwell, J. W.; Cheatham, T. E., III.; Wang, J.; Ross, W. S.; Simmerling, C. L.; Darden, T. A.; Merz, K. M.; Stanton, R. V.; Cheng, A. L.; Vincent, J. J.; Crowley, M.; Tsui, V.; Gohlke, H.; Radmer, R. J.; Duan, Y.; Pitera, J.; Massova, I.; Seibel, G. L.; Singh, U. C.; Weiner, P. K.; Kollman, P. A. AMBER7; University of California, San Francisco: San Francisco, CA, 2002.
(25) Rocchia, W.; Sridharan, S.; Nicholls, A.; Alexov, E.; Chiabrera, A.; Honig, B. *J. Comput. Chem.* **2002**, *23*, 128.
(26) Gilson, M. K.; Sharp, K. A.; Honig, B. H. *J. Comput. Chem*. **1987**, *9*, 327.
(27) The initial effective free energy starts at −954 kcal/mol. The first transient plateau appears between 500 ps and 1 ns, and the averaged effective free energy in this period is −1004 kcal/mol.
(28) Duan, Y.; Kollman, P. A. *Science* **1998**, *282*, 740.
(29) O'Neil, K. T.; DeGrado, W. F. *Science* **1990**, *250*, 646.
(30) Chakrabartty, A.; Baldwin, R. L. Stability of α-helices. *Adv. Protein Chem.* **1995**, *46*, 141.
(31) Horton, N.; Lewis, M. *Protein Sci.* **1992**, *1*, 169.
(32) Wells, J. A. *Proc. Natl. Acad. Sci. U. S. A.* **1996**, *93*, 1.
(33) Kutzki, O.; Park, H. S.; Ernst, J. T.; Orner, B. P.; Yin, H.; Hamilton, A. D. *J. Am. Chem. Soc.* **2002**, *124*, 11838.
(34) Ernst, J. T.; Becerril, J.; Park, H. S.; Yin, H.; Hamilton, A. D. *Angew. Chem., Int. Ed. Engl.* **2003**, *42*, 535.
(35) DINO: Visualizing Strucutural Biology (**2002**) http://www.dino3d.org.
(36) We performed the cluster analysis using the Charmm program[37] version c28b1. In the cluster analysis using angle data, we set the cluster group radius and max error equal to 20 and 0.001.
(37) Brooks, B. R.; Bruccoleri, R. E.; Olafson, B. D.; States, D. J.; Swaminathan, S.; Karplus, M. *J. Comput. Chem*. **1983**, *4*, 187.
(38) Guijarro, J. I.; Jackson, M.; Chaffotte, A. F.; Delepierre, M.; Mantsch, H. H.; Goldberg, M. E. *Biochemistry* **1995**, *34*, 2998.